ADVANCED OPTICAL MATERIALS
www.advopticalmat.de

Reversible Three-Dimensional Focusing of Visible Light with Ultrathin Plasmonic Flat Lens

Xianzhong Chen, Lingling Huang, Holger Mühlenbernd, Guixin Li, Benfeng Bai, Qiaofeng Tan, Guofan Jin, Cheng-Wei Qiu, Thomas Zentgraf,* and Shuang Zhang**

Metasurfaces with interfacial phase discontinuities provide a unique platform for manipulating light propagation both in free space and along a surface. Three-dimensional focusing of visible light is experimentally exhibited as a bi-functional phenomenon by controlling the radial orientation of identical plasmonic dipoles, generating a desired phase profile along the interface. With this technique, the in-plane and out-of-plane refractions are manipulated by an ultrathin flat lens such that a beam can be focused into a 3D spot either in a real or virtual focal plane, which can be reversed via manipulation of the circularly polarized status of the incident light. Both the inverted real image and the upright virtual image of an arbitrary object are experimentally demonstrated using the same flat lens in the visible range, which paves the way towards robust application of phase discontinuity devices.

1. Introduction

As engineered artificial materials, metamaterials usually gain their properties from structure rather than composition, and have properties that may not be found in nature.[1–6] A novel type of metamaterial consisting of only a monolayer of thin plasmonic artificial atoms exhibiting interfacial phase discontinuities—so-called 'metasurfaces'—have recently attracted enormous interest.[7–19] Metasurfaces typically consist of a planar array of plasmonic antennas with carefully designed shapes and orientations to generate a desired phase profile along the interface. A plethora of plasmonic devices based on this new concept have been experimentally demonstrated in visible[11,12] and infrared wavelengths.[7–10] Notably, polarization-dependent directional surface plasmon polariton excitation using a metasurface with phase discontinuity has been experimentally demonstrated.[16,17] An abrupt phase discontinuity introduced by a monolayer of plasmonic structures has been used in developing plasmonic lenses operating at telecom[10] and terahertz[13] ranges. These ultrathin plasmonic metalenses differ dramatically from traditional lenses, which function either by controlling the surface topography or varying the spatial profile of the refractive index.

Among all the applications of metasurfaces, one interesting development is a plasmonic metalens exhibiting dual polarities (e.g., convex for right circularly polarized (RCP) incident light and concave for left circularly polarized (LCP) incident light, or vice versa)[12] at visible and near infrared range. Polarization controlled phase discontinuities were introduced for circularly polarized (CP) light, which enables construction of a metalens to converge or diverge the input CP light depending on the helicity of the input light. This is in contrast to previously demonstrated plasmonic lens,[10,13] where the phase discontinuity occurs for the conversion between two linear polarization states. In principle, phase-discontinuity metasurfaces[7–11] and metalenses[10,13] all exploit the phase manipulation via a planar surface containing nanoparticles.[9] Hence a surface with appropriate dielectric gratings can also accomplish a similar functionality of metasurfaces[7,8] or bi-functionality of metalenses,[12] provided that the spatially varying grating provides a local twist to the phase of transmitted light.[20]

The dual-polarity metalens demonstrated previously[12] only manipulated the light along one direction owing to one-directional phase variation by the dipole array, resulting in distortion of the image of an arbitrary object due to the different magnifications along two directions. Here we demonstrate an ultrathin flat lens with polarization dependent radial phase variation to display three-dimensional focusing spots either in the real or the virtual focal plane. In particular, we demonstrate the formation of both real and virtual images of an object by changing the

Dr. X. Chen, L. Huang, Prof. S. Zhang
School of Physics & Astronomy
University of Birmingham
Birmingham, B15 2TT, UK
E-mail: ioechenxiz@gmail.com; s.zhang@bham.ac.uk
L. Huang, Prof. B. Bai, Prof. Q. Tan, Prof. G. Jin
State Key Laboratory of Precision Measurement Technology and Instruments
Department of Precision Instrument
Tsinghua University
Beijing, 100084, China
H. Mühlenbernd, Prof. T. Zentgraf
Department of Physics
University of Paderborn
Warburger Straße 100, D-33098, Paderborn, Germany
E-mail: thomas.zentgraf@upb.de
Dr. G. Li
Department of Physics
Hong Kong Baptist University, Hongkong
Prof. C.-W. Qiu
Department of Electrical and Computer Engineering
National University of Singapore
4 Engineering Drive 3, Singapore, 117576, Singapore

DOI: 10.1002/adom.201300102

FULL PAPER

circular polarization of the input beam (i.e., RCP or LCP). The imaging properties of such a flat lens are investigated for an object located both within and outside the focal plane.

2. Results

2.1. Design and Fabrication of the Lens

Methods for phase control have been described previously.[11,12] Briefly, the phase shift, ranging from 0 to 2π, is realized by a metasurface consisting of plasmonic dipoles with spatially varying orientation angles ϕ. The local abrupt phase change is governed by the relation $\phi = \pm 2\varphi$, with the sign determined by the combination of the incidence/transmission polarizations.[12] This phase change can be considered as the Pancharatnam–Berry (PB) phase that is acquired when the polarization state of light travels around a contour on the Poincare sphere.[21,22] Specifically, for an incident beam with circular polarization σ, the phase difference between the scattered waves of opposite circular polarization σ– scattered by two dipole antennas of different orientations ϕ_1 and ϕ_2 can be viewed as half of the solid angle enclosed between two paths on the Poincare sphere, $\sigma\rightarrow L(\phi_1)\rightarrow\sigma$–, and $\sigma\rightarrow L(\phi_2)\rightarrow\sigma$–, where σ and σ- are represented by the north and south poles of the Poincare sphere, and $L(\phi_i)$ are the linear polarization states residing on the equator of the Poincare sphere.[21] Interestingly, the PB phase would be reversed if the polarizations of the incident and scattered waves are exchanged. Thus, by controlling the helicity of the input and detected CP light, the sign of the phase discontinuity can be readily reversed. In order to focus a circularly polarized incident plane wave, a phase shift needs to be introduced at the metasurface which varies with the radius from the optic axis (r). This can be realized by using dipole antennas with spatially varying orientations. To achieve the phase profile equivalent to a conventional two-dimensional lens, the following expression governs the relation between the rotation angle ϕ and the location of dipole antenna:

$$\varphi(r) = \pm 0.5 k_0 \left(\sqrt{f^2 + r^2} - |f|\right) \tag{1}$$

where $k_0 = 2\pi/\lambda$ is the free space wave vector, f is the focal length of the lens, and r is the distance to the origin. The '+' and '–' sign in Equation (1) corresponds to a positive and negative polarity, respectively, for a right circularly polarized (RCP) incident wave, while the opposite definition applies to a left circularly polarized (LCP) incident wave.

As shown by **Figure 1**a, the metalens is composed of dipole antennas arranged in a number of evenly spaced concentric rings, with the radius of the rings increasing by a step size of 400 nm. Within each ring, the dipole antennas have the same orientation and the separation between two neighboring dipoles along the ring is 400 nm. The antenna structures are defined in a resist film by using standard electron beam lithography. Thereafter, a 40 nm gold film is deposited via thermal evaporation. The lens structures are obtained by a lift-off procedure. An scanning electron microscopy (SEM) image of the resulting patterns for the lens (left) designed at a wavelength of 740 nm and the corresponding phase shift profile (right) are shown in Figure 1b. The lenses have a diameter of 180 µm with a focal length $f = 80$ µm. Each dipole antenna is 200 nm long and 50 nm wide (shown in Figure 1a).

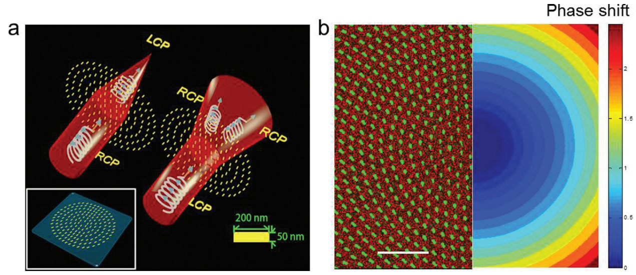

Figure 1. Schematic of a metalens with interchangeable polarity and an SEM image of the fabricated plasmonic lens. (a) The focusing properties of the same metalens can be switched between a convex lens and a concave lens by controlling the helicity of the incident light. Each dipole antenna is 200 nm long and 50 nm wide. (b) SEM image of the fabricated two-dimensional dual-polarity plasmonic lens (top view) with a focal length of 80 µm (left). The corresponding phase shift profile is displayed on the right. The dipoles that are arranged on the same annulus have the same orientation. The distance between two neighboring annuluses is 400 nm along both the radial and azimuth directions. The scale bar is 2 µm.

2.2. Characterization of the Lens

We first characterize the focusing performance of the metalens with a laser beam at $\lambda = 740$ nm. By gradually tuning the distance between an objective lens and the plasmonic metalens, the optical intensity distribution is examined along the propagation direction to determine the focal point. **Figure 2** shows the microscope image of the metalens illuminated by white light (Figure 2a) and the focal point at the focal plane (Figure 2b) by using the laser beam. From the intensity distribution of the laser beam at the focal plane (Figure 2c), a focused spot with a diameter of 7.2 µm at full width of half maximum is experimentally obtained.

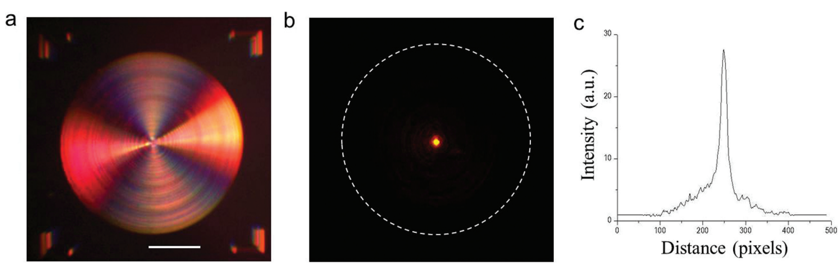

Figure 2. Optical microscope images of (a) the metalens illuminated with white light and (b) the focal point at real focal plane illuminated with a RCP incident laser beam at 740 nm. The scale bar is 50 µm. The position of the lens is marked by the white dashed circles. (c) Experimental measurement of the intensity distribution at the focal plane along one direction. Each pixel is equal to 0.37 µm. The spot diameter at full width of half maximum is 7.2 µm.

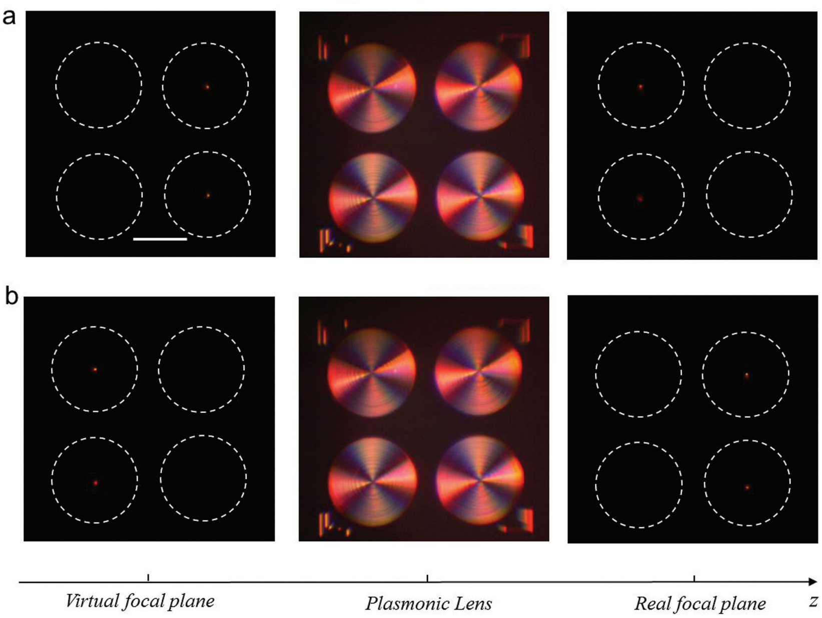

Figure 3. Lens polarity is switched by changing the helicity of the incident light. Optical microscope images at virtual focal plane (left), lens surface (middle) and real focal plane (right) for the incident light with (a) RCP and (b) LCP. The scale bar is 50 µm. CP laser beam is incident on the lenses from the left along the z direction, with the lens located at z = 0. Positions of lenses are marked by the white dashed circles. The polarity of the two lenses on the left is different from that of the lenses on the right for the same CP light.

To validate the reversible polarity of such circular phase-discontinuity lens, four metalenses are fabricated side by side, including two positive lenses on the left and two negative lenses on the right for RCP incident light. **Figure 3** shows the optical microscopy images for two different incident/transmission polarization combinations: RCP/LCP (Figure 3a) and LCP/RCP (Figure 3b). As shown by Figure 3a (left) for the RCP incident beam, we observe two bright focal points for the lenses on the right at $z = -80$ µm, which are virtual focal points as they lie on the incident side of the plasmonic lens. This confirms that lenses on the right are negative (concave) for the incident light with RCP polarization. On the other hand, two real focal points on the transmission side of the plasmonic lens at z = 80 µm are observed for the two lenses on the left. As shown in Figure 3b, when the circular polarizations of the incident and transmitted beam are interchanged, the focusing behavior for all the lenses is reversed, unambiguously verifying that switching in the focusing properties from positive (negative) to negative (positive) is solely attributed to the helicity change of the CP for the incident and transmitted light.

We further study the imaging functionality of such circular metalenses. The lens used for imaging has a diameter of 80 µm and a focal length of 80 µm, and its polarity is positive for RCP incident light. The object to be imaged consists of an array of "T" apertures with a pitch of 20 µm along both in-plane directions (shown in **Figure** 4a), which are fabricated on a chromium film with a thickness of 50 nm. Each 'T' aperture is designed with a height of 11 µm and a width of 6 µm. The object and metalens are separated by an air gap whose thickness is controlled by the spacers at the edge of the samples.

For an object distance greater than the focal length of the metalens, it is expected that an inverted real image is formed for a positive (convex) lens. This is confirmed by the measurement with an object distance of 150 µm with RCP incident light, where the metalens functions as a positive lens (Figure 4b). By comparing with the image of the "T" patterns without the plasmonic lens, the magnification of the image formed by the metalens can be obtained. Experimentally, we measured the magnification of the image to be 1.3, which shows reasonable agreement with a simple ray calculation of 1.14. The slight difference in magnification is due to the substrate flatness and air gap accuracy. Due to the resolution limitation of the measurement system, the

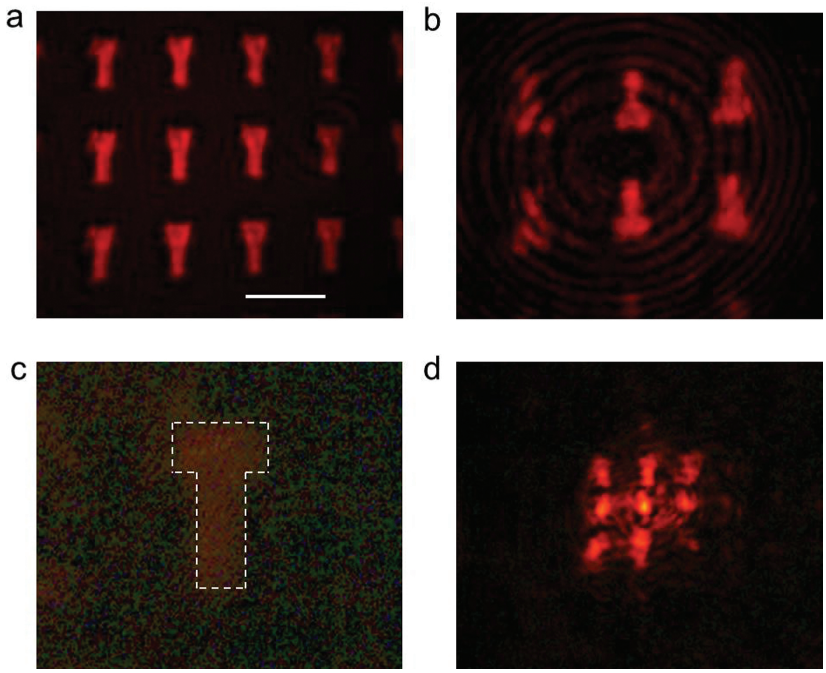

Figure 4. Experimental demonstration of imaging. (a) A "T" pattern array with a pitch of 20 µm along both in-plane directions is used as an object. The scale bar is 20 µm. The object and the lens are separated by an air gap whose thickness is controlled by spacers at the edge of the samples. (b) A real and inverted image with a magnification of 1.3 is achieved for RCP incident light, in which the polarity of lens is positive (convex lens). The air gap is 150 µm. (c) A virtual and upright image with a magnification of 3.1 on a positive lens with an air gap of 55 µm. The edge of the image is marked by the white dashed lines. (d) For the same air gap as in (c), a virtual and upright image with a magnification of 0.58 is obtained when switching the incident light from RCP to LCP, with the polarity of the same lens being negative (concave lens).

upright virtual image for LCP incident light with a predicted magnification of 0.34 cannot be resolved.

In order to observe the upright virtual image, we decrease the air gap to 55 μm. As the air gap is within the focal length of the plasmonic metalens, upright virtual images are observed for both circular polarizations of incident light, as shown in Figure 4c,d. The magnifications in Figure 4c and d are 3.1 and 0.58, respectively, which coincide with the magnification of 3.2 for positive lens (convex) with RCP incident light, and magnification of 0.59 for the negative lens (concave) with LCP incident light. Thus, the reconfigurable imaging functionality of the same plasmonic metalens as a convex lens or a concave lens is clearly demonstrated by controlling the helicity of the incident CP light.

3. Discussion

The conversion efficiency between two circular polarization states is an important parameter in the performance of the lens. In our presented work the conversion efficiency between the focused power and the incident power is measured around 5%. With further optimization of the design parameters, for example, by increasing the density of the dipoles, and better alignment of the resonance wavelength of the antennas to the operating wavelength of the lens, the dipole antennas can achieve a significantly higher transmission in the converted polarization. Considering that scattering of the dipole antenna is evenly split between left handed and right handed circular polarizations, and further split equally along the transmission and reflection directions, the upper limit of efficiency is 25% if the material loss is neglected. If each unit cell consists of two orthogonal dipoles with detuned resonance frequencies and consequently a significant phase difference, there will be a constructive interference for conversion from one circular polarization to the other, and the conversion efficiency can be further enhanced.[15] The image quality is mainly determined by the quality of the fabricated sample and the measurement system. By minimizing the fabrication error and defects (e.g. missing dipoles) during the fabrication process and optimizing the imaging system, the image quality will be greatly improved.

4. Conclusion

Here we have experimentally realized a polarity reversible circular flat metalens operating at visible frequencies. The unambiguous evidence of lens focusing shows that the CP light can be converged into a real 3D spot or diverged to form a virtual 3D spot by one identical flat plasmonic lens. The polarity of the same lens is interchangeable by controlling the helicity of the incident and transmitted beams. For the first time, the inverted real images and the upright virtual images of an arbitrary object without distortion are experimentally demonstrated on the same dual-polarity metalens in the visible range. Such two-dimensional plasmonic metalenses are an important step toward practical applications of switchable flat aberration-free lensing, empowered by phase discontinuity.

5. Experimental Section

A poly methyl methacrylate resist layer is spin-coated on the ITO coated glass substrate and baked on a hotplate at 150 °C for 10 min to remove the solvent. The antenna structures are defined in the resist by using standard electron beam lithography, followed by a lift-off procedure. The optical measurement setup includes multiple lenses, two quarter-wave plates, two linear polarisers, an objective, and a charge coupled device (CCD) camera. The incident CP light and the opposite circular polarization in transmission are generated by a quarter-wave plate and a polariser on each side of the plasmonic lens. To measure the transmitted light with opposite helicity to that of incident light, the polarization directions of the two polarisers are oriented parallel to each other. The distance between an object and the metalens is controlled by a spacer with different thickness inserted between them. A 20×/0.40 objective to collect the scattering light after the sample is mounted on a three-dimensional stage. To image an object, light from a laser source at a wavelength of 740 nm is incident on the backside of the lens. By moving the stage and controlling the position of a CCD camera, the transmission through the sample (object and plasmonic lens) is collected with the objective and imaged on the CCD camera.

Acknowledgements

This work is partly supported by the Engineering and Physical Sciences Council of the United Kingdom. T. Z. and S. Z. acknowledge the financial support by the European Commission under the Marie Curie Fellowship Program. B. Bai and L. Huang acknowledge the support by the National Natural Science Foundation of China (Projects No. 61227014, No, 11004119, and No.61161130005) and the Ministry of Science and Technology of China (Project No.2011BAK15B03). L. H. acknowledges the Chinese Scholarship Council (CSC, No. 2011621202) for financial support. T. Z. and H. M. acknowledge the support by the DFG Graduate Program GRK 1464 "Micro and Nanostructures in Optoelectronics and Photonics". C.W.Q. acknowledges the partial support by the National University of Singapore (Project No. R-263–000–688–112).The authors thank Professor R. Palmer for use of the Nanoscale Physics Research Laboratory Cleanroom and Dr A. Robinson for useful conversations. The Oxford Instruments PlasmaPro NGP80 Inductively Coupled Plasma etching system used in this research was obtained through the Birmingham Science City project "Creating and Characterising Next Generation Advanced Materials" supported by Advantage West Midlands (AWM) and partially funded by the European Regional Development Fund (ERDF).

Received: February 1, 2013
Revised: May 1, 2013
Published online: May 26, 2013

[1] B. Edwards, A. Alu, M. G. Silveirinha, N. Engheta, *Phys. Rev. Lett.* **2009**, *103*, 153901.
[2] R. A. Shelby, D. R. Smith, S. Schultz, *Science* **2001**, *292*, 77.
[3] J. Valentine, S, Zhang, T. Zentgraf, E. Ulin-Avila, D. A. Genov, G. Bartal, X. Zhang, *Nature* **2008**, *455*, 376.
[4] N. Fang, H. Lee, C. Sun, X. Zhang, *Science* **2005**, *308*, 534.
[5] J. Valentine, J. Li, T. Zentgraf, G. Bartal, X. Zhang, *Nat. Mater.* **2009**, *8*, 568.
[6] T. Ergin, N. Stenger, P. Brenner, J. B. Pendry, M. Wegener, *Science* **2010**, *328*, 337.
[7] N. Yu, P. Genevet, M. A. Kats, F. Aieta, J.-P. Tetienne, F. Capasso, Z. Gaburro, *Science* **2011**, *334*, 333.
[8] X. Ni, N. K. Emani, A. V. Kildishev, A. Boltasseva, V. M. Shalaev, *Science* **2012**, *335*, 27.
[9] N. Engheta, *Science* **2011**, *334*, 317–318.

[10] F. Aieta, P. Genevet, M. A. Kats, N. Yu, R. Blanchard, Z. Gaburro, F. Capasso, *Nano Lett.* **2012**, *12*, 1702.
[11] L. Huang, X. Chen, H. Mühlenbernd, G. Li, B. Bai, Q. Tan, G. Jin, T. Zentgraf, S. Zhang, *Nano Lett.* **2012**, *12*, 5750.
[12] X. Chen, L. Huang, H. Mühlenbernd, G. X. Li, B. Bai, Q. Tan, G. Jin, C. W. Qiu, S. Zhang, T. Zentgraf, *Nature Commun.* **2012**, *3*, 1198.
[13] D. Hu, X. Wang, S. Feng, J. Ye, W. Sun, Q. Kan, P. J. Klar, Y. Zhang, *Adv. Optical Mater.* **2013**, *1*, 186.
[14] X. Yin, Z. Ye, J. Rho, Y. Wang, X. Zhang, *Science* **2013**, *339*, 1405.
[15] M. Kang, T. Feng, H.-T. Wang, J. Li, *Opt. Exp.* **2012**, *20*, 15882.
[16] J. Lin, J. P. Balthasar Mueller, Q. Wang, G. Yuan, N. Antoniou, X.-C. Yuan, F. Capasso, *Science* **2013**, *340*, 331.
[17] L. Huang, X. Chen, B. Bai, Q. Tan, G. Jin, T. Zentgraf, S. Zhang, *Light: Sci. Applications* **2013**, *2*, e70.
[18] S. Sun, Q. He, S. Xiao, Q. Xu, X. Li, L. Zhou, *Nat. Mater.* **2012**, *11*, 426.
[19] S. Sun, K.-Y. Yang, C.-M. Wang, T.-K. Juan, W. T. Chen, C. Y. Liao, Q. He, S. Xiao, W.-T. Kung, G.-Y. Guo, L. Zhou, D. P. Tsai, *Nano Lett.* **2012**, *12*, 6223.
[20] E. Hasman, V. Kleiner, G. Biener, A. Niv, *Appl. Phys. Lett.* **2003**, *82*, 328.
[21] M. V. Berry, *J. Mod. Opt.* **1987**, *34*, 1401.
[22] S. Pancharatnam, *Proc. Indian Acad. Sci. A* **1956**, *44*, 247.